BJR

Received: 5 November 2013 | Revised: 16 January 2014 | Accepted: 3 February 2014

doi: 10.1259/bjr.20130716

Cite this article as:
Lu L, Xu K, Zhang LJ, Morelli J, Krazinski AW, Silverman JR, et al. Lung ischaemia–reperfusion injury in a canine model: dual-energy CT findings with pathophysiological correlation. Br J Radiol 2014;87:20130716.

FULL PAPER

Lung ischaemia–reperfusion injury in a canine model: dual-energy CT findings with pathophysiological correlation

[1,2]L LU, [2]K XU, [1]L J ZHANG, [3]J MORELLI, [4]A W KRAZINSKI, [4]J R SILVERMAN, [4]U J SCHOEPF and [1]G M LU

[1]Department of Medical Imaging, Jinling Hospital, Medical School of Nanjing University, Nanjing, China
[2]The Affiliated Hospital of Xuzhou Medical College, Xuzhou, China
[3]Department of Radiology, Scott and White Memorial Hospital, Temple, TX, USA
[4]Department of Radiology and Radiological Science, Medical University of South Carolina, Charleston, SC, USA

Address correspondence to: Dr Guang Ming Lu
E-mail: cj.luguangming@vip.163.com

Li Lu and Kai Xu both contributed equally to this article.

Objective: To evaluate dual-energy CT (DECT) findings of pulmonary ischaemic–reperfusion injury (PIRI) and its pathophysiological correlation in the canine model.
Methods: A PIRI model was established in 11 canines, utilizing closed pectoral balloon occlusion. Two control canines were also included. For the PIRI model, the left pulmonary artery was occluded with a balloon, which was deflated and removed after 2 h. DECT was performed before, during occlusion and at 2, 3 and 4 h thereafter and was utilized to construct pulmonary perfusion maps. Immediately after the CT scan at the fourth hour post reperfusion, the canines were sacrificed, and lung specimens were harvested for pathological analysis. CT findings, pulmonary artery pressure and blood gas results were then analysed.
Results: Data at every time point were available for 10 animals (experimental group, $n = 8$; control group, $n = 2$). Quantitative measurements from DECT pulmonary perfusion maps found iodine attenuation values of the left lung to be the lowest at 2 h post embolization and the highest at 1 h post reperfusion. In the contralateral lung, perfusion values also peaked at 1 h post reperfusion. Continuous hypoxia and acid–based disorders were observed during PIRI, and comprehensive analysis showed physiological changes to be worst at 3 h post reperfusion.
Conclusion: DECT pulmonary perfusion mapping demonstrated pulmonary perfusion of the bilateral lungs to be the greatest at 1 h post reperfusion. These CT findings corresponded with pathophysiological changes.
Advances in knowledge: DECT pulmonary perfusion mapping can be used to evaluate lung ischaemia–reperfusion injury.

Ischaemia–reperfusion injury (IRI) occurs under a variety of clinical conditions, including lung and/or cardiac transplantation, cardiopulmonary bypass, pulmonary resection, re-expansion pulmonary oedema, shock, cardiopulmonary resuscitation and pulmonary embolism.[1–3] Pulmonary embolism is a common cause of pulmonary IRI (PIRI), and the incidence of pulmonary embolism is increasing[4,5] with a mortality rate of up to 30%.[6] With timely identification and treatment of pulmonary embolism, mortality rates can be reduced to <10%.[7] However, reperfusion after treatment for lung ischaemia can also cause serious complications, such as haemorrhage and pulmonary oedema.[8] Therefore, it is important to understand both the pathophysiological and imaging appearances of pulmonary IRI. Lung transplantation is also a common cause for PIRI following pulmonary arterial occlusion. Currently, the incidence of PIRI following transplantation is estimated at up to 25%. Post transplantation, PIRI can lead to insufficiency of the primary lung graft, delayed graft function, acute or chronic rejection (*e.g.* pulmonary oedema and acute respiratory failure), and increased early post-operative mortality and graft failure.[9,10]

CT is currently the predominant modality for the imaging assessment of thoracic disorders, including PIRI. Dual-energy CT (DECT) allows simultaneous acquisition of dual-energy data sets, allowing for decomposition of the scanned entity based on differences in attenuation between air, soft tissue and iodine.[11] One application of this principle in pulmonary imaging is the ability to obtain iodine maps demonstrating the distribution of pulmonary perfusion. The use of CT perfusion mapping has been shown to be relatively sensitive and highly specific for the detection of pulmonary emboli.[12]

Figure 1. CT scans of lungs of an experimental canine at different time points. (a) The lungs were clear prior to embolization. (b) Left lung markings were decreased at 2 h post occusion, whereas the right lower lobe demonstrated slight ground-glass opacifications (GGOs). (c–f) Images obtained at 1, 2, 3 and 4 h post reperfusion(hpr); respectively, demonstrated various degrees of bilateral GGOs with the most extensive findings in this case obtained at 3 hpr (e). In this case, more extensive GGOs were present on the left lung.

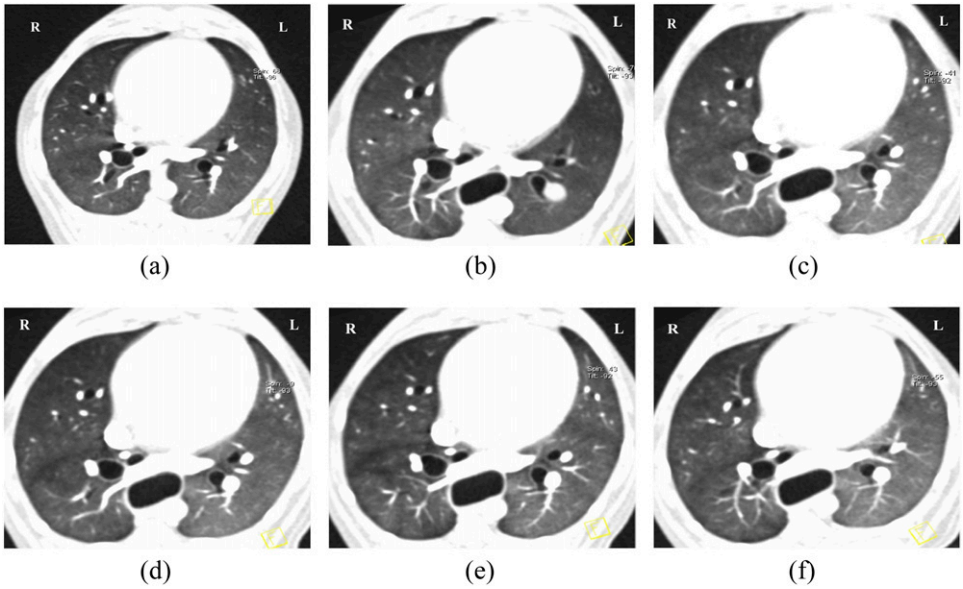

Recent research into PIRI has focused on the pathological and molecular biological mechanisms.[13–16] To date, there are few reports on imaging and pathophysiological findings in PIRI.[17,18] CT perfusion findings in PIRI have also not yet been described. The aim of this study was to assess PIRI imaging and pathophysiological findings in a canine model.

METHODS AND MATERIALS

Model preparation

The study protocol was approved by our local animal care committee and performed in accordance with institutional guidelines. A total of 13 healthy adult canines of mixed genetic background, weighing 20–23 kg, were included in this study. The canines were randomly assigned to either an experimental ($n = 11$) or a control group ($n = 2$).

Experimental group

6- to 8-ml of ketamine (Fujian Kutian Pharmaceutical Co. Ltd Ningde City, China) was administered to the canines via intramuscular injection. Propofol (AstraZeneca, Milan, Italy) was used (2 ml per trial) to maintain anaesthesia. The animals were not intubated, and each animal's heart and respiratory rates were allowed to vary freely. No specific measures were taken to prevent atelectasis. After the administration of anaesthesia, the animals were placed in a supine position for performance of non-contrast CT imaging. This was done to assess the presence of atelectasis and other pulmonary parenchymal pathology. After this scan, fur was removed from the left hindlimb, and the superficial vein was punctured with a trocar. The trocar was fixed after sealing with heparin, stabilizing the access route for anaesthesia and a high-pressure syringe. Skin of the bilateral groin areas was sterilized with an iodine tincture (2.5%). A 3-cm longitudinal incision running along the course of the femoral artery, 2 cm deep into the inguinal ligament, was then cut to separate the skin, fascia and muscle, and expose the femoral artery and vein. The femoral artery and vein were punctured using the Seldinger technique with a 5 French catheter sheath group (Cordis Corporation,Atlanta, GA). The femoral artery access was used for drawing blood for blood gas analysis. The femoral vein access was utilized for collection of venous blood for routine blood testing and for accessing the pulmonary arteries. The right arteria cervicalis superficialis was punctured using the same method. The distal catheter was placed in the main pulmonary artery under the guidance of digital subtraction angiography (DSA; GE innova 3100DSA, GE Healthcare, Fairfield, CT) with a connected T-tube. This was used to measure pulmonary artery pressure and to perform pulmonary arteriography (contrast agent dose was 27 ml with a flow rate at 5 ml s^{-1}). Then, a balloon (8 × 40 mm; Cordis Corporation) was inserted into the left inferior pulmonary artery from the femoral vein under DSA access. Balloon markers were located under fluoroscopic guidance. Prior to balloon occlusion, intravenous heparin was administered in each canine (10 ml, 1% heparin solution) to prevent thrombosis distal to the created pulmonary artery occlusions. 2 ml of saline was utilized to inflate each balloon after confirmation of correct placement.

Control group

For the control group, the experimental steps were identical, except that normal saline was not injected into the balloon after insertion into the left inferior pulmonary artery.

Figure 2. Evidence of successful occlusion and subsequent recanalization. (a–c) Pulmonary angiography images before, during and after left pulmonary artery occlusion performed under digital subtraction angiography guidance. (a) The arrow demonstrates widely patent pulmonary arteries prior to embolization. (b) The left pulmonary artery was not visible after balloon inflation in the artery. (c) After the balloon was deflated, the left pulmonary artery was again visible. (d–f) CT pulmonary angiogram (CTPA) images of pulmonary maximum intensity projections and (g–i) CTPA three-dimensional reconstructions demonstrate analogous findings; (d, g) bilateral pulmonary arteries and their branches were widely patent before embolization; (e, h) successful occlusion; (f, i) successful recanalization without evidence of emboli. L, left; R, right.

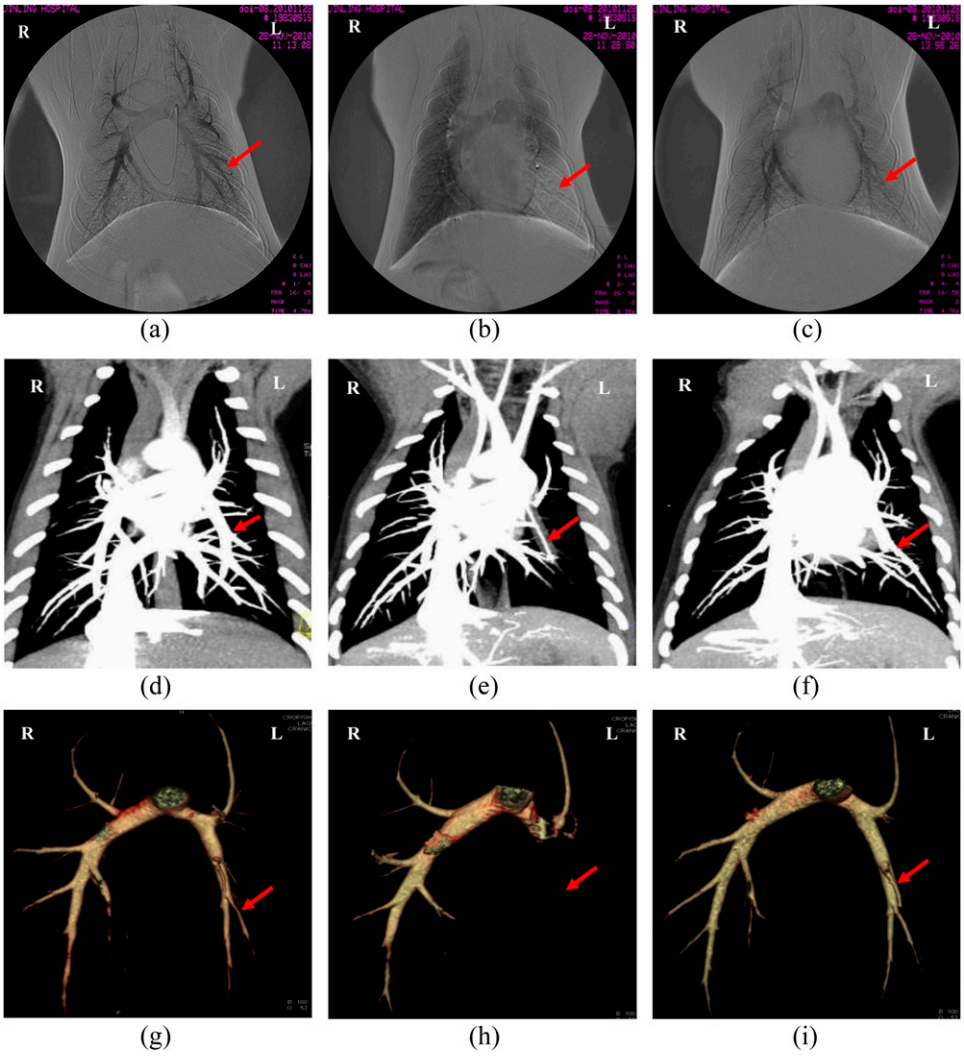

CT imaging technique

CT scanning and analysis

All scans were performed with a dual source CT scanner (Somatom® Definition, Siemens, Forchheim, Germany); scans were performed before embolization, 2 h post occlusion (hpo) of the left inferior pulmonary artery, and 1, 2, 3 and 4 h post reperfusion (hpr). The detector width (260 mm field of view) included the entire lung of each canine. The scan direction was cranial to caudal. The non-contrast CT scans were acquired using the following parameters: tube voltage of 120 kVp, tube current of 130 mA, collimator width of 32 × 0.6 mm, gantry rotation time of 0.5 s per rotation, pitch of 1.4, scan field of view of 255 × 255 mm, slice thickness of 0.75 mm and scan time of 6.09 s. A helical acquisition was performed for scanning in dual-energy mode. The region of interest (ROI) was set in the main pulmonary artery. When the density within the ROI reached 100 HU (delay time was approximately 6 s), DECT scanning was begun, performed with the following parameters: tube A voltage of 140 kVp, tube A effective current of 51 mAs, tube B voltage of 80 kVp, tube B effective current of 213 mAs, collimator width of 32 layers × 0.6 mm, gantry rotation time of 0.33 s per rotation, pitch of 0.9, scan field of view of 337 × 337 mm, thickness of 0.75 mm, automatic reconstruction interval of 0.5 mm and a scan time of 5.72 s. The injection dose of contrast agent (370 mgI ml^{-1} iopamidol; Shanghaibo Lecco Xinyi Pharmaceutical Co., Ltd Shanghai, China) was 30 ml with a flow rate of 3.0 ml s^{-1}. Contrast media injection was followed by injection of 15 ml of saline bolus chaser at 3.0 ml s^{-1}. This was done to reduce the residual contrast agent in the superior vena cava. The data were

Figure 3. Dual-energy CT pulmonary perfusion maps at different time points. (a) Perfusion in both lungs was uniform before embolization. (b) The left lung showed obvious perfusion defects at 2 h post occlusion. (c–f) Respective 1, 2, 3 and 4 h post reperfusion images demonstrate reperfusion. HU, Hounsfield units; L, left; R, right.

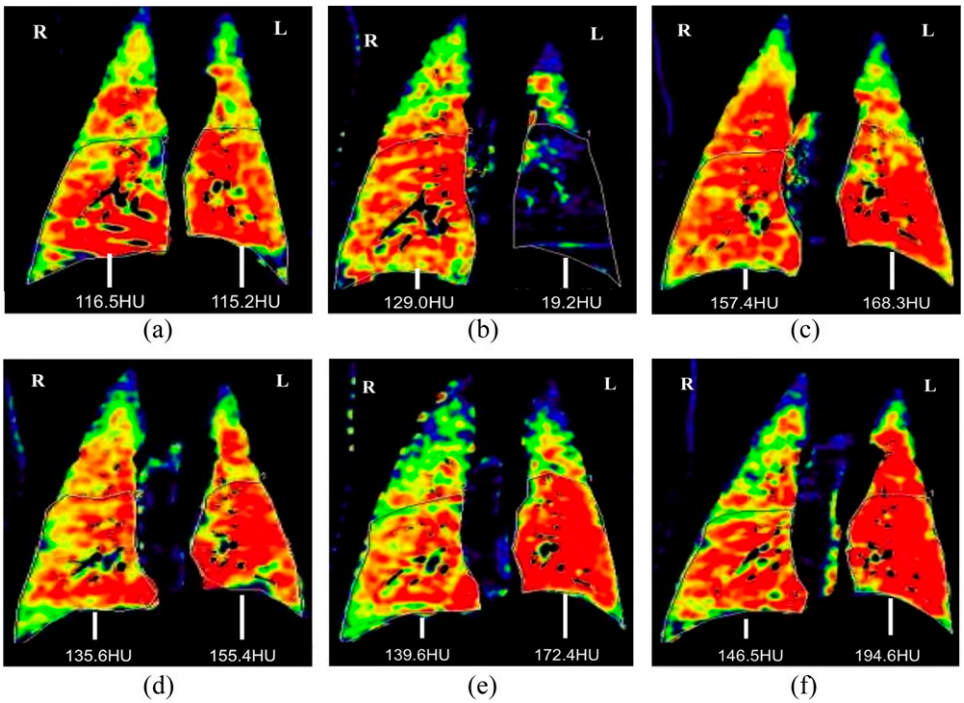

automatically transmitted to the workstation when the scan was completed. The raw data were automatically reconstructed as three groups of data with 0.75 mm slice thickness (80, 140 and 80/140 kVp fused images in the ratio of 3:7).

Dual-energy CT analysis

Two radiologists with 10 and 4 years' chest CT experience evaluated DECT manifestations of PIRI in the bilateral pulmonary parenchyma at each time point above. The data were analysed at a workstation (Syngo MMWP VE31A; Siemens Medical Solutions, Forchheim, Germany) with perfused blood volume dual-energy lung perfusion imaging software to display images for CT pulmonary angiogram (CTPA), dual-energy perfusion imaging (DEPI) and fused CTPA–DEPI images. The DEPI software constructs maps of iodine attenuation, the degree of which directly corresponds to the degree of pulmonary arterial perfusion present. All series were reviewed in horizontal, coronal and sagittal planes. CT value ranges, as calculated by DEPI, were −960 to −200 HU. All data were displayed using the same threshold range before and after embolization. The pseudocolours for lung perfusion were 16-bit greyscale and positron emission tomography (PET) rainbow 16-bit. The colour distribution denoted variations in lung perfusion with red colours representing areas of high perfusion and blue representing areas of low perfusion. ROIs were placed in the left and right lower lobes of the lungs on the DEPI to determine Hounsfield units of these areas on iodine maps in coronal, sagittal and axial images utilizing the Freehand ROI tool. The readers also assessed CT findings present on the 80/140 kVp fused images acquired. The presence and laterally of such findings were described according to standard terminology.[19] Atelectasis was defined as reduced lung volumes with associated attenuation increases in the associated portions of the lung. A consolidation was defined as homogeneously increased parenchymal opacity obscuring visualization of bronchovascular structures. Ground-glass opacities were similar but less opaque and without obscuration of such structures. A mosaic attenuation pattern consisted of patchy areas of differential attenuation. The observers were asked to judge at which time points the abnormalities identified were first detected and on which side the abnormalities were most extensive.

Measurement of pulmonary arterial pressure

The distal end of the vena cervicalis catheter was attached to the PX260 pressure sensor (Edwards Lifesciences, LLC Irvine, CA), which was connected to the ECG monitor (SIRECUST 960 ECG monitor, Siemens). Pulmonary artery mode was chosen after opening the T-tube. Then, pulmonary arterial systolic pressure (PASP), pulmonary arterial diastolic pressure (PADP) and pulmonary arterial mean pressure (PAMP) were measured in real time. The results were recorded before embolization, at 2 hpo, and at 1, 2, 3 and 4 hpr.

Blood gas analysis

Blood samples were obtained from the femoral artery and vein, for blood gas analysis (GEM® Premier 3000 Instrumentation Laboratory Company, Lexington, MA) and routine blood tests (Sysmex XE-2100 blood cell analyser TOA Medical Electronics, Kobe, Japan), respectively. The canines' real-time rectal temperature was measured before each extraction. The fractional concentration of inspired oxygen was set to 21%. The indices of analysis included oxygen partial pressure (pO_2), pH value,

Table 1. Hounsfield units of dual-energy CT pulmonary perfusion iodine map images at different time points

Groups	Lung	Before embolism	2 hpo	1 hpr	2 hpr	3 hpr	4 hpr	*F* value	*p*-value
Experimental ($n = 8$)	Left[a]	73.07 ± 16.75	14.06 ± 3.03	137.22 ± 18.16	113.00 ± 39.85	121.65 ± 34.99	132.62 ± 50.96	21.300	0.001
	Right	98.93 ± 13.20	119.53 ± 22.24	133.02 ± 27.78	112.23 ± 35.17	125.83 ± 26.28	128.51 ± 32.04	12.100	0.033
Control ($n = 2$)	Left	95.20 ± 0.42	92.65 ± 17.89	107.75 ± 28.21	105.50 ± 4.95	118.10 ± 5.52	117.30 ± 15.84	0.966	0.505
	Right	103.10 ± 0.98	110.15 ± 10.54	110.45 ± 18.74	112.20 ± 9.05	104.45 ± 8.98	106.75 ± 20.01	0.155	0.971

Data shown as mean ± standard deviation.
hpo, hours post occlusion; hpr, hours post reperfusion.
[a]Occlusion of the (inferior) pulmonary artery.

Figure 4. Hounsfield units reflecting iodine content from CT dual-energy perfusion imaging (DEPI) of the bilateral lungs at different time points. Hounsfield units of the left lung DEPI images were the lowest at 2 h post occlusion (hpo) and the highest at 1 h post reperfusion (hpr). In this case, Hounsfield unit values of the right lung began to increase at 2 hpo, peaking at 1 hpr. HU, Hounsfield units; L, left; R, right.

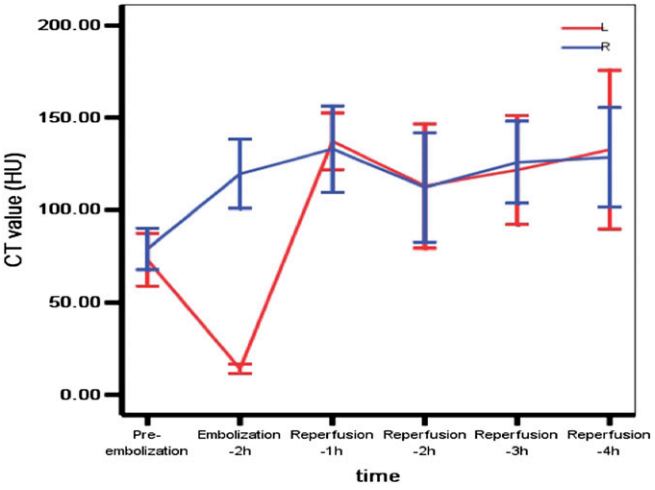

carbon dioxide partial pressure (pCO_2), total carbon dioxide, actual and standardized bicarbonate concentrations, base excess of whole blood (BE), lactic acid concentration, arterial blood oxygen saturation (SaO_2), alveolar blood pO_2, alveolar blood pO_2 difference and arterial blood pO_2 ratio. The blood gas analysis results were recorded and analysed before embolization, at 2 hpo, and at 1, 2, 3, and 4 hpr.

Histological analysis

After the final CT scan, the canines were sacrificed by ketamine overdose administration via the femoral vein. The lungs were dissected, flushed with saline and fixed in 10% formaldehyde solution. Next, haematoxylin and eosin (H&E) staining was performed. Pathological findings were observed in tissue sections with a light microscope. For electron microscopy preparation, lung tissues were immobilized in a mixed solution of 6% glutaraldehyde and 1% osmium tetroxide, and then dehydrated stepwise in acetone. The lung tissue was sectioned into thinner slices (<0.1 μm) and stained with uranyl acetate and lead citrate. The sections were evaluated using a transmission electron microscope (JEOL JEM-1011; JEOL Ltd, Tokyo, Japan).

Statistical analysis

All statistical analyses were performed using SPSS® v. 13.0 software package (SPSS, Inc., Chicago, IL). Quantitative data were provided as mean ± standard deviations, while qualitative data were given as rates and percentages. Homogeneity of variance testing was performed on CT values, pulmonary arterial pressures and blood gas analysis results at the six time points for each lung. Single factor analysis of variance was used if the variance was homogeneous, while a non-parametric test of a number of independent samples was used when the variance was heterogeneous. When differences were statistically significant, the least

Table 2. Pulmonary artery pressure at different time points (mmHg)

Pulmonary artery pressure	Before embolism	2 hpo	1 hpr	2 hpr	3 hpr	4 hpr	*F* value	*p*-value
PASP	24.38 ± 7.80	26.50 ± 6.99	21.25 ± 7.46	20.25 ± 7.46	24.00 ± 8.49	22.13 ± 9.49	0.685	0.638
PADP	5.25 ± 4.89	11.63 ± 6.39	9.75 ± 8.17	8.25 ± 7.32	9.50 ± 7.82	10.75 ± 9.59	0.715	0.616
PAMP	14.50 ± 5.48	19.25 ± 4.10	15.13 ± 6.60	14.25 ± 6.18	15.75 ± 7.05	16.38 ± 9.38	0.604	0.697

hpo, hours post occlusion; hpr, hours post reperfusion; PADP, pulmonary artery diastolic pressure; PAMP, mean pulmonary artery pressure; PASP, pulmonary artery systolic pressure.
Data shown as mean ± standard deviation.

significant difference method was used for pairwise comparisons between groups. *p*-values <0.05 were considered statistically significant.

RESULTS

Model preparation

Of the 11 canines in the experimental group, 10 successfully underwent pulmonary ischaemia–reperfusion procedure and subsequent imaging; 1 died due to anaesthesia complications. Data from two canines in the experimental group were not included in the analysis because the CT values, pulmonary artery pressures and blood gas analysis results were not available at 4 hpr, as this information was lost when the data were uploaded to the picture archiving and communication system.

CT findings

Non-contrast CT findings indicated no abnormalities in the lungs of the eight experimental and two control canines prior to the procedures. At 2 hpo, mosaic attenuation was found in the lungs of all eight experimental canines with predominantly decreased attenuation involving the left lower lobes. The right lungs in these animals demonstrated ground-glass opacification (GGO) to various degrees. During reperfusion, GGOs were identified within the bilateral lungs of the eight canines. No other abnormalities were present, and there was no definite trend to the changes observed in the lung contralateral to the occlusion. Qualitatively, bilateral GGOs were first detected at various time points post reperfusion ($n = 7$); two canines developed lesions at 1 hpr, one canine at 2 hpr, three canines at 3 hpr and one canine at 4 hpr. The other canine developed bilateral GGOs at 2 hpo, but the opacities resolved on reperfusion. All other GGOs were still detectable at 3 and 4 hpr ($n = 7$). Comprehensive evaluation of all time points showed that left-sided GGOs were (slightly) more extensive than those in the right lung in four canines, whereas the right-lung lesions were (slightly) more severe in the other four canines. In the control group, bilateral lungs were clear, and no GGOs or other pulmonary abnormalities were identified on any of the acquired CT images. Figure 1 demonstrates typical lung window findings from one experimental canine assessed at the six evaluated time points. No atelectasis, consolidations or other findings were detected at any time point for any of the evaluated animals.

Figure 5. Pulmonary artery pressure maps at different time points. Pulmonary arterial systolic pressure (PASP), pulmonary arterial diastolic pressure (PADP) and pulmonary arterial mean pressure (PAMP) are increased at 2 h post occlusion but decreased at 1 and 2 h post reperfusion. Pulmonary artery pressures are elevated again at 3 or 4 h after reperfusion, but they did not restore to pre-embolization levels.

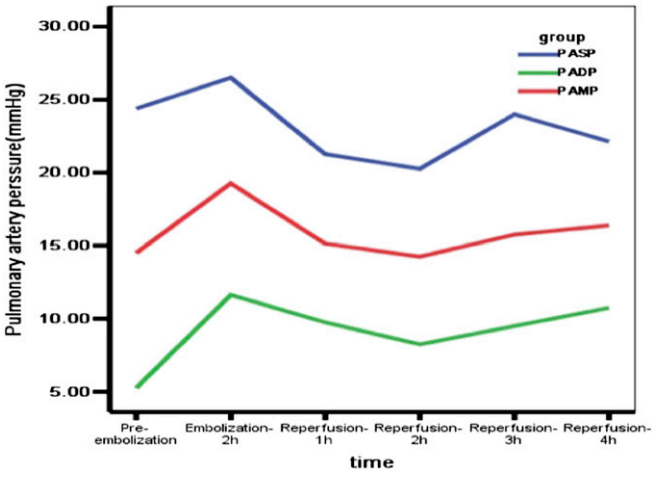

Figure 2a–c illustrate DSA images acquired before pulmonary artery occlusion, during occlusion and following reperfusion. Figure 2d–f show maximum intensity projections obtained from dual-energy CTPA at similar time points. Figure 2g–i are dual-energy CTPA images at the aforementioned time points. The bilateral pulmonary arteries and their branches were displayed clearly before occlusion (Figure 2a,d,g). The left inferior pulmonary artery was not observed during the balloon occlusion procedure (Figure 2b,e,h). After deflation of the balloon, the left inferior pulmonary artery was perfused without evidence of distal emboli (Figure 2c,f,i). Figure 3 was derived from DEPI at different time points. These images indicated obvious perfusion defects in the left lung at 2 hpo (Figure 3b) as well as uniform perfusion in both lungs before balloon occlusion (Figure 3a) and after reperfusion (Figure 3c–f).

As shown in Table 1, a statistically significant difference was found in the perfusion images for pre- and post-occlusion Hounsfield unit in both left and right lungs ($p < 0.05$). CT values of the left lung reached a minimum at 2 hpo and a maximum at 1 hpr. The maximum Hounsfield unit of the right lung were present at 1 hpr. Figure 4 shows the trend of increasing Hounsfield unit values on

Table 3. Blood gas analysis results at different time points

Indices	Before embolism	2 h after embolism	1 h after reperfusion	2 h after reperfusion	3 h after reperfusion	4 h after reperfusion	*F* value	*p*-value
pO_2 (mmHg)	102.33 ± 40.43	90.44 ± 19.90	95.44 ± 11.62	92.67 ± 10.34	83.67 ± 18.67	87.67 ± 10.49	0.829	0.535
pCO_2 (mmHg)	40.22 ± 9.95	32.67 ± 9.49	31.33 ± 8.14	29.44 ± 8.57	34.00 ± 7.60	33.56 ± 6.80	1.679	0.158
SaO_2 (%)	93.44 ± 5.80	93.44 ± 9.60	96.11 ± 1.17	96.00 ± 1.41	91.67 ± 8.31	94.44 ± 3.00	3.385 (χ^2)	0.641
Alveolar BOPP difference (mmHg)	11.56 ± 21.22	18.78 ± 17.73	7.44 ± 10.19	12.89 ± 10.96	17.44 ± 16.06	17.44 ± 10.11	0.771	0.575
Alveolar BOPP (mmHg)	100.44 ± 12.95	108.78 ± 11.90	108.89 ± 9.27	111.22 ± 10.49	105.89 ± 9.21	107.11 ± 8.22	1.129	0.358
Arterial BOPP ratio	0.89 ± 0.22	0.83 ± 0.17	0.93 ± 0.09	0.89 ± 0.09	0.83 ± 0.16	0.84 ± 0.09	0.741	0.596
BE ($mmoll^{-1}$)	−8.49 ± 1.95	−9.90 ± 2.57	−10.06 ± 2.08	−10.71 ± 3.48	−11.40 ± 2.46	−10.97 ± 3.24	1.321	0.271
HCO_3^- ($mmoll^{-1}$)	18.33 ± 1.56	17.00 ± 1.87	16.89 ± 1.45	16.33 ± 2.55	15.67 ± 2.00	16.44 ± 2.55	1.588	0.181

BE, base excess of whole blood; BOPP, blood oxygen partial pressure; pCO_2, carbon dioxide partial pressure; pO_2, oxygen partial pressure; SaO_2, oxygen saturation.
Data shown as mean ± standard deviation.

DEPI images obtained at different time points. No statistically significant differences were observed in pre- or post-procedural CT values for either left or right lungs in the control group ($p > 0.05$).

Pulmonary arterial pressure

Table 2 shows the results of pulmonary artery pressure measurements at different time points. There was no statistically significant difference ($p > 0.05$) among pulmonary artery pressures at the six time points, including PASP ($F = 0.68$, $p = 0.638$), PADP ($F = 0.715$, $p = 0.616$) and PAMP ($F = 0.604$, $p = 0.697$). However, PASP, PADP and PAMP were elevated at 2 hpo, decreased at 2 hpr and gradually increased thereafter. Figure 5 depicts pulmonary artery pressure changes mapped by time point.

Blood gas analysis

Table 3 shows blood gas analysis results at different time points. There were no significant differences ($p > 0.05$) among the values of pCO_2, pO_2, lactic acid, total amount of carbon dioxide, actual concentration of bicarbonate, standard concentration of bicarbonate, BE, SaO_2, alveolar blood pO_2 difference, alveolar blood pO_2 or arterial blood pO_2 ratios. The pO_2 increased and pCO_2 decreased between 2 hpo and 1 hpr. The lowest pO_2 appeared at 3 hpr accompanied by an elevated pCO_2. Both pO_2 and pCO_2 did not rebound to pre-occlusion levels until 4 hpr. At 3 hpr, the mean values of alveolar blood pO_2 difference were the highest, while the alveolar blood pO_2 was the lowest, indicating the worst pulmonary ventilation function for that time. BE was the lowest at 3 hpr, indicating severe acidosis. SaO_2 reached a minimum at 3 hpr. Comprehensive review of blood gas analysis results suggested that the body was in an uncompensated state of severe hypoxia and acid–base imbalance at 3 hpr.

Histological analysis

Assessment of gross specimens and H&E staining indicated pathological changes of the left lung to be more severe than those of the right in 4 out of the 8 animals, and vice versa in the remainder. This corresponded to the extent of GGOs observed on CT. A typical gross specimen is illustrated in Figure 6a along with H&E stains (Figure 6b,c). These demonstrate dark red and oedematous pulmonary tissue on the ischaemic side (*i.e.* the left) but only scattered, punctate dark red areas in the right side (Figure 6a). H&E stained images of the ischaemic side, post reperfusion, showed pulmonary capillary dilatation and congestion, focal alveolar haemorrhage, alveolar atelectasis and widened alveolar septa (Figure 6b). There were also widened alveolar septa in the right side, although the pathological changes were less severe. Electron microscopy images of tissue from the ischaemic region of the left lower lobe of one canine, post reperfusion, indicated alveolar epithelial cell degeneration (epithelial cells stripped to the alveolar space, Figure 7a), congestion of alveolar septum, capillary endothelial cell degeneration and mitochondrial vacuolization. The right lower lobe pulmonary tissue from this canine also demonstrated alveolar epithelial cell degeneration, mitochondrial vacuolization (Figure 7b) and scattered tissue cells and macrophages. There were pseudoinclusion bodies in nuclei, alveolar epithelial exfoliation, and, occasionally, neutrophils (Figure 7c) in the superior aspect of the obtained pulmonary tissue.

Figure 6. (a) Gross specimens with corresponding haematoxylin and eosin (H&E) staining 200×. (b–c) In this case, H&E staining of the same specimen indicates that pathological changes of the left (L) lung were more severe than those of the right (R) lung. The gross specimens (a) and H&E staining images demonstrate red and oedematous lung tissue in the L. However, there were only scattered punctate findings in the R side. (b) In the L lung, H&E staining images show pulmonary capillary dilatation and congestion, focal alveolar haemorrhage (arrow), alveolar atelectasis (rectangle) and widened alveolar septa on the L. (c) In the R lung, there are also widened alveolar septa (rectangle) in the side, although the pathological changes are not obvious as on the L.

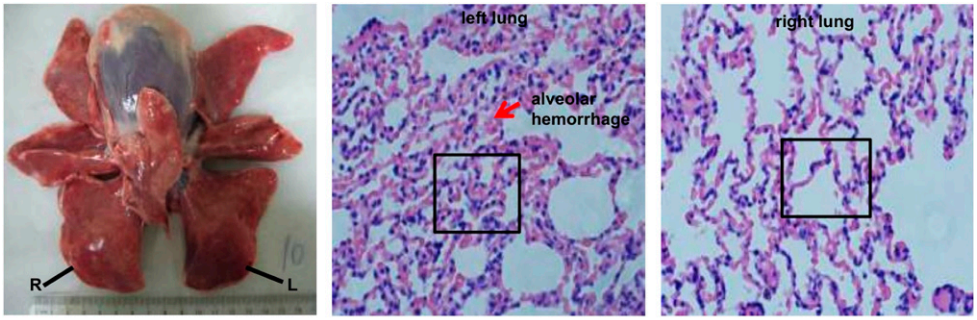

DISCUSSION

The present study describes for the first time DECT and CT perfusion abnormalities of normal lung following experimentally induced IRI in a canine model with pathological correlation. When the left lower lobe pulmonary artery was occluded, decreased perfusion was, as expected, quantitatively present on DEPI within the left lower lobe. On reperfusion, GGOs were noted bilaterally, GGOs were greater on the left for half of the cases and were greater on the right for the other half. These corresponded with pathological changes observed that similarly appeared to be worse on the left in half of the animals and on the right in the other half. With DEPI, an increase in bilateral pulmonary perfusion over baseline was observed with reperfusion. GGOs persisted until 4 h post reperfusion in all but one subject. Physiological parameters worsened over time after reperfusion.

PIRI consists of ischaemia and reperfusion, both of which can cause cell damage. Thoma et al[20] found that acute pulmonary emboli can cause non-ischaemic lung GGO due to partial filling of airspaces, thickening of the interstitium (blood, cells and fibres), collapse of the alveoli and/or increased capillary blood flow. These factors lead to inadequate ventilation and ultimately to hypoxaemia. In this study, during reperfusion, the bilateral lungs of eight canines showed varying degrees of GGO that persisted for 4 h in all but one case. The pulmonary perfusion, as shown by DEPI, was quantitatively the greatest at 1 hpr. This may have resulted from damage to the capillary endothelium and subsequent alterations in vascular permeability.[21] CT perfusion Hounsfield unit did not normalize to a baseline level at 4 hpr but remained elevated. Values for pO_2 were the lowest and pCO_2 the highest at 3 hpr, which suggests that the canines were becoming hypoxic at this point. Supporting this, SaO_2 was also at a minimum, the difference between the average alveolar and arterial oxygen pressure was the greatest, and the alveolar blood oxygen pressure was the smallest at this time point. These factors suggest that pulmonary ventilation was at its worst at this time point. The measured BE was also the lowest at 3 hpr, suggesting that the canines, were in a state of acidosis.

The pulmonary vasculature theoretically responds to hypoxia in a manner opposite to other regions of the body, such as the brain parenchyma. Hypoxia causes small pulmonary arteries to

Figure 7. (a) Transmission electron microscope (TEM) images of one canine. TEM image shows alveolar epithelial cell degeneration (epithelial cells stripped to the alveolar space, arrow) of tissue in ischemia–reperfusion region of left lower lung. (b) TEM image of the right lower lung shows cytoplasmic degeneration, capillary endothelial cell degeneration and mitochondrial vacuolization (arrow). (c) Neutral granulocytes (arrow) are seen in the right upper lung as well.

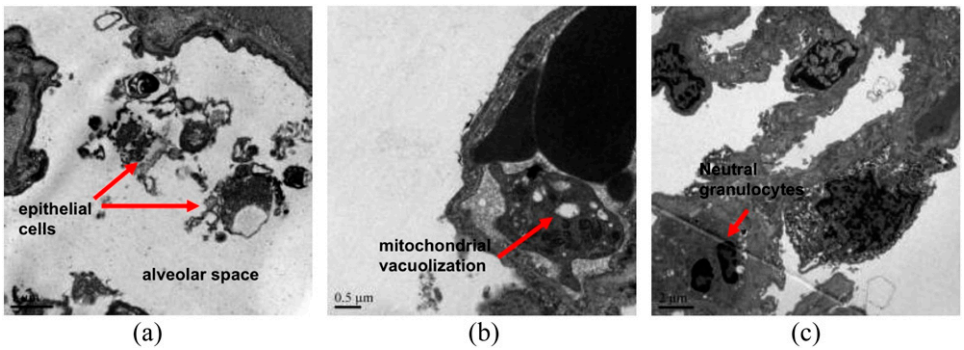

contract, as is reflected by the high PASP at 3 hpr. However, this value was still lower than the PASP prior to arterial occlusion. During the early phases of reperfusion (1 and 2 hpr), pulmonary artery pressure was reduced. This may relate to a protective mechanism by which pulmonary arterial pressure is reduced to diminish mechanical damage to the vascular endothelial cells by blood flow–shear stress. According to the images and pathophysiological findings, manifestations of PIRI were most severe at 3 hpr. This suggests that extra caution and preventative measures should be taken clinically in patients approaching 3 hpr. Watanabe et al[22] mentioned that because of the vasospasm and micro thrombi in the ischaemic lung, inflammatory mediators and factors in the blood could cause parenchymal damage in the lung contralateral to arterial occlusion/embolization. This was seen in every case in this study, both pathologically and by imaging appearance. Findings were most severe on the left in half of the subjects and on the right in the other half. The release of inflammatory mediators and reactive oxygen species (ROS) are therefore likely to contribute to injury not only in the local region affected by occlusion but also within the contralateral lung via their systemic circulation. That is, the injury of the lung contralateral to the occluded vascular segment was likely caused by systemic spread of humoral factors, such as ROS, thromboxane, cytokines and other inflammatory mediators/factors produced by PIRI.[23] Some of these could thus reach the contralateral lung and induce damage. As in similar prior studies,[22] this work found that the left pulmonary artery occlusion and reperfusion had an impact on the non-ischaemic right lung at 4 hpr. Therefore, prolonging the observation time of reperfusion would be beneficial to the study of PIRI to determine precisely when CT and perfusion abnormalities resolve.

The PIRI model can be implemented either *in vivo* or *ex vivo* in isolated lung preparations. However, isolated lung preparations present some disadvantages to reproducing PIRI. The main disadvantage is that systemic neurohumoral factors are removed. Therefore, this method cannot truly reproduce the pathological processes involved in PIRI. The use of *in vivo* models realistically reproduces the pathophysiological changes of PIRI. Two methods are usually used to create *in vivo* models, either clamping or ligation of the pulmonary artery via an open procedure or balloon embolization in the closed chest. The injury associated with the open-chest model increases premature mortality rate. In addition, some operations that are part of the thoracotomy, such as cutting of the ribs, opening the pericardium, separating the pulmonary arteries and re-expanding the lungs can result in injury of the chest, affecting the outcome of the PIRI analysis. With *in vivo* balloon embolization, there is no need for thoracotomy and fewer injuries to surrounding tissues are produced. In addition, the occlusion and reperfusion can be easily controlled, further enabling *in vivo* simulation of clinical pulmonary reperfusion. This study successfully produced a PIRI model in a canine model using the closed pectoral balloon embolization method. The success rate was 92.3% (12/13), with one death due to inappropriate anaesthesia, rather than a surgical complication.

One additional concern in the development of a PIRI model is selection of an appropriate duration of pulmonary arterial occlusion. The lungs are perfused by two separate vascular systems:[24] the pulmonary circulation for gas exchange and the bronchial circulation for delivery of oxygen and nutrients to the airway proximal to the respiratory bronchioles. Normally, the blood of the bronchial artery only comprises 1–2% of the cardiac output. Occlusion of the pulmonary vasculature for an extended time will lead to a compensatory expansion of the bronchial artery, so it is important to select appropriate occlusion duration. Liu et al[25] occluded a pulmonary artery and measured the indices of blood flow at different time points (0.5, 1, 2 and 4 h). They found that the safest pulmonary artery occlusion time without resultant fatal lung injury was 2 h. Thus, for the present study, 2 h was chosen as the reperfusion time point. This is similar to the time frame employed during lung transplantation surgery. Although, other previous studies have demonstrated that ligation of pulmonary arteries could cause pathological changes of the lungs within only 1 h of embolization.[26]

Our study had several limitations. Although the control group experiments confirmed no obvious effect of the repeated administration of contrast agents on the CT or CT perfusion images and parameters, such an influence cannot be entirely excluded. Experimental complexity limited our observations of the changes of ischaemia–reperfusion to 4 hpr. Since pulmonary GGOs and perfusion abnormalities were still present at this time point, in future studies the observation time of the reperfusion process should be extended to aid further understanding of lung IRI. The present study also did not evaluate pathological specimens at 1, 2 or 3 hpr, and pulmonary arterial pressure and blood gas were not measured for the control group. Experimental animal models are intrinsically limited; although, analogous experiments would be very difficult to perform clinically. In terms of model selection, both canines and pigs tolerate such procedures well; however, the structure of lung tissues, distribution of pulmonary segments and vasculature morphology of canines are more similar to humans,[27] and canines are more cost effective. Compared with rats and rabbits, the vasculature of canines and pigs are thicker, which is better suited for interventional procedures. Thus, canines were ultimately selected for our animal model.

In summary, this study demonstrated a high success rate in implementing a closed pectoral balloon occlusion model in canines to reproduce the pathophysiological processes and imaging findings of PIRI. This model demonstrated bilateral lower lobe GGO to be the predominant pathological finding in PIRI, persisting for at least 4 h after the occlusive event. Additionally, pulmonary perfusion was significantly increased both on ischaemic and non-ischaemic sides as assessed by DECT. These findings were consistent with pathophysiological changes observed, such as increases in pulmonary capillary permeability, dilatation and congestion of vessels, hypoxaemia and disruption of acid–base balance.

CONFLICT OF INTERESTS

UJS is a consultant for and receives research support from Bayer, Bracco, GE, Medrad and Siemens. The other authors have no conflicts of interest to declare.

FUNDING

This work was partially supported by the Program for New Century Excellent Talents in University (NCET-12-0260).

REFERENCES

1. Lu YT, Hellewell PG, Evans TW. Ischemia–reperfusion lung injury: contribution of ischemia, neutrophils, and hydrostatic pressure. *Am J Physiol* 1997; **273**: L46–54.
2. Takeyoshi I, Tanahashi Y, Aiba M, Sunose Y, Iwazaki S, Tsutsumi H, et al. Spontaneous nitric oxide (FK409) ameliorates pulmonary ischemia-reperfusion injury in dogs. *Transplant Proc* 2000; **32**: 2428–9.
3. Zhang LJ, Zhao YE, Wu SY, Yeh BM, Zhou CS, Hu XB, et al. Pulmonary embolism detection with dual-energy CT: experimental study of dual-source CT in rabbits. *Radiology* 2009; **252**: 61–70. doi: 10.1148/radiol.2521081682
4. Lu GM, Wu SY, Yeh BM, Zhang LJ. Dual-energy computed tomography in pulmonary embolism. *Br J Radiol* 2010; **83**: 707–18. doi: 10.1259/bjr/16337436
5. Fujinaga T, Nakamura T, Fukuse T, Chen F, Zhang J, Ueda S, et al. Isoflurane inhalation after circulatory arrest protects against warm ischemia reperfusion injury of the lungs. *Transplantation* 2006; **82**: 1168–74.
6. Ng CS, Wan S, Yim AP. Pulmonary ischaemia–reperfusion injury: role of apoptosis. *Eur Respir J* 2005; **25**: 356–63. doi: 10.1183/09031936.05.00030304
7. den Hengst WA, Gielis JF, Lin JY, Van Schil PE, De Windt LJ, Moens AL. Lung ischemia-reperfusion injury: a molecular and clinical view on a complex pathophysiological process. *Am J Physiol Heart Circ Physiol* 2010; **299**: 1283–99. doi: 10.1152/ajpheart.00251.2010
8. Laack TA, Goyal DG. Pulmonary embolism: an unsuspected killer. *Emerg Med Clin North Am* 2004; **22**: 961–83. doi: 10.1016/j.emc.2004.05.011
9. Tapson VF. Acute pulmonary embolism. *N Engl J Med* 2008; **358**: 1037–52. doi: 10.1056/NEJMra072753
10. Edagawa M, Yoshida E, Matsuzaki Y, Shibuya K, Shibata K, Onitsuka T, et al. Reduction of post-ischemic lung reperfusion injury by fibrinolytic activity suppression. *Transplantation* 1999; **67**: 944–9.
11. Kang MJ, Park CM, Lee CH, Goo JM, Lee HJ. Dual-energy CT: clinical applications in various pulmonary diseases. *Radiographics* 2010; **30**: 685–98. doi: 10.1148/rg.303095101
12. Thieme SF, Becker CR, Hacker M, Nikolaou K, Reiser MF, Johnson TR. Dual energy CT for the assessment of lung perfusion: correlation to scintigraphy. *Eur J Radiol* 2008; **68**: 369–74. doi: 10.1016/j.ejrad.2008.07.031
13. Kasahara M, Takeyoshi I, Ohwada S, Sunose Y, Iwazaki S, Aiba M, et al. Effect of FK3311 on ischemia–reperfusion injury in canine pulmonary models. *Transplant Proc* 2000; **32**: 2430–1.
14. Wolf PS, Merry HE, Farivar AS. Stress-activated protein kinase inhibition to ameliorate lung ischemia reperfusion injury. *J Thorac Cardiovasc Surg* 2008; **135**: 656–65. doi: 10.1016/j.jtcvs.2007.11.026
15. Townsley MI, Morisseau C, Hammock B, King JA. Impact of epoxyeicosatrienoic acids in lung ischemia–reperfusion injury. *Microcirculation* 2010; **17**: 137–46. doi: 10.1111/j.1549-8719.2009.00013.x
16. Marom EM, Choi YW, Palmer SM, DeLong DM, Stuart MD, McAdams HP. Reperfusion edema after lung transplantation: effect of daclizumab. *Radiology* 2001; **221**: 508–14. doi: 10.1148/radiol.2212010381
17. Kundu S, Herman SJ, Winton TL. Reperfusion edema after lung transplantation: radiographic manifestations. *Radiology* 1998; **206**: 75–80. doi: 10.1148/radiology.206.1.9423654
18. Amundsen T, Kvaerness J, Aadahl P, Waage A, Bjermer L, Odegård A, et al. A closed-chest pulmonary artery occlusion/reperfusion model in the pig: detection of experimental pulmonary embolism with MR angiography and perfusion MR imaging. *Invest Radiol* 2000; **35**: 295–303.
19. Hansell DM, Bankier AA, MacMahon H, McLoud TC, Müller NL, Remy J. Fleischner Society: glossary of terms for thoracic imaging. *Radiology* 2008; **246**: 697–722. doi: 10.1148/radiol.2462070712
20. Thoma P, Rondelet B, Mélot C, Tack D, Naeije R, Gevenois PA. Acute pulmonary embolism relationships between ground-glass opacification at thin-section CT and hemodynamics in pigs. *Radiology* 2009; **250**: 721–9. doi: 10.1148/radiol.2503081134
21. Chen KH, Chao D, Liu CF, Chen CF, Wang D. Ischemia and reperfusion of the lung tissues induced increase of lung permeability and lung edema is attenuated by dimethylthiourea (PP69). *Transplant Proc* 2010; **42**: 748–50. doi: 10.1016/j.transproceed.2010.03.016
22. Watanabe A, Kawaharada N, Kusajima K, Komatsu S, Takahashi H. Contralateral lung injury associated with single-lung ischemia–reperfusion injury. *Ann Thorac Surg* 1996; **62**: 1644–9.
23. Farivar AS, Delgado MF, McCourtie AS, Barnes AD, Verrier ED, Mulligan MS. Crosstalk between thrombosis and inflammation in lung reperfusion injury. *Ann Thorac Surg* 2006; **81**: 1061–7. doi: 10.1016/j.athoracsur.2005.09.047
24. Matute-Bello G, Frevert CW, Martin TR. Animal models of acute lung injury. *Am J Physiol Lung Cell Mol Physiol* 2008; **295**: L379–399. doi: 10.1152/ajplung.00010.2008
25. Liu H, Wang Z, Zhang J, Wu H, Yin R, Xu B, et al. Temporarily pulmonary hilum clamping as a thoracic damage-control procedure for lung trauma in swine. *J Trauma* 2010; **68**: 810–17. doi: 10.1097/TA.0b013e3181b16d15
26. Zhang LJ, Chai X, Wu SY, Zhao YE, Hu XB, Hu YX, et al. Detection of pulmonary embolism by dual energy CT: correlation with perfusion scintigraphy and histopathological findings in rabbits. *Eur Radiol* 2009; **19**: 2844–54. doi: 10.1007/s00330-009-1518-z
27. Brandes H, Albes JM, Conzelmann A, Wehrmann M, Ziemer G. Comparison of pulsatile and nonpulsatile perfusion of the lung in an extracorporeal large animal model. *Eur Surg Res* 2002; **34**: 321–9. doi: 10.1159/000063067